AN EMPIRICAL CRITERION FOR LAMINAR-TO-TURBULENT BOUNDARY-LAYER TRANSITION

By Richard Eppler, Stuttgart, Germany

Presented at the XXV OSTIV Congress, Saint Auban, France

Abstract

A simple empirical criterion for prediction of the laminar-to-turbulent transition in boundary layers is presented. It considers the instability history of the boundary layer without evaluating the amplification rates of the linear instability theory. Because the instability history also influences the size of the laminar separation bubbles, it was also possible to develop an empirical evaluation of the drag increase due to separation bubbles. Several examples demonstrate the capabilities of the procedure.

1. Introduction

Laminar-to-turbulent boundary-layer is a process with several phases. It does not occur at a precise location. Intensive research has been devoted to this problem during our century. Although many details are understood, it is still impossible to predict the location where the turbulent boundary layer begins. A short summary of the present state of the art illustrates the difficulties. Only two-dimensional boundary layers are considered.

1. Every boundary layer is initially laminar. A local Reynolds number is a significant parameter, for example,

$$R_{\delta_2} = \frac{U\delta_2}{\nu} \qquad (1)$$

which is based on the local potential-flow velocity U, the momentum thickness δ_2, and the kinematic viscosity ν. If R_{δ_2} increases during the development of the boundary layer, the flow becomes unstable above a critical value R_N of R_{δ_2}. Certain disturbances, Tollmien-Schlichting (TS) waves, are then amplified. Boundary layers in favorable pressure gradients have higher R_N values than those in adverse pressure gradients.

Linear stability theory can be considered complete. However, this theory is limited to very small amplitudes of the TS waves.

2. If the amplitude of the unstable TS waves increases, nonlinear effects cause higher harmonics of the first wave that, in many cases, are not amplified further.

3. The planview of the linear TS waves is straight. A secondary instability was found that causes a wavy deformation of the waves in the planview. The theory of this secondary instability is again limited to small deformations.

4. The secondary instabilities develop much more quickly than the primary ones. They soon lead to Λ-shaped vortex formations in which layers with very high shear are present. This has been found in experiments and in predictions by means of "direct numerical simulation," i.e., numerical solutions of the Navier-Stokes equations.

5. Near the high-shear layers, new high-frequency disturbances can grow rapidly. These disturbances lead to local turbulent spots.

6. The turbulent spots spread and eventually form the turbulent boundary layer.

Phases 2 to 6 have been the subject of intensive theoretical and experimental research during the last three decades. This research concerns the mechanisms that lead to turbulence. However, only the amplification rates and the later development are known. All theories and experiments introduce well-defined, initial disturbances. It remains unknown from which disturbances natural transition develops. Moreover, other mechanisms may lead to turbulence that are still unknown. These are the reasons why the transition location still cannot be predicted even though some transition mechanisms are known. Transition prediction is, therefore, still a matter of empirical criteria.

There are many so-called local criteria that are based on the fact that R_{δ_2} and a shape factor H define the magnitude of the instability of laminar boundary layers. Normally, many experimental results are plotted in a diagram $R_{\delta_2}(H)$. This yields a certain cloud of points that shows clear tendencies. Some average curves can be found that can be used as transition criteria $R_{\delta_2}(H)$. These criteria are very simple because R_{δ_2} and H are known during the evaluation of the boundary layer. Such local criteria have been widely used. It is, however, clear that they do not consider the instability history of the boundary layer. The local transition criterion can be met after a very long or a very short instability history. This is a weak point of the local criteria.

Other criteria have, therefore, been developed that consider the instability history. The most well-known class of such criteria is the so-called e^N-criteria. They consider linear stability theory by calculating, for many TS waves, the total amplification. If one of the amplifications reaches the value e^N, transition is assumed to occur. The value of N is determined from experiments. Different values have been used from $N = 7$ to $N = 13$.

This type of criteria is surely better than the local criteria because they consider the first phase of the transition process. They are, however, much more complicated because many TS waves must be evaluated. Most of them are initially amplified and later damped. Those waves that finally reach an amplification of e^N mostly develop rapidly. A long part of the instability history is thus neglected. The same is true for the nonlinear production of higher harmonics.

A new criterion has, therefore, been developed that is very simple and more empirical, but still considers the instability history. It is described in the present paper.

2. Definitions

A two-dimensional flow around a contour, a wing of infinite span, is supposed. The cross section of the contour has an arc length s, measured on both sides from the stagnation point. The contour is located in an infinite, parallel flow with the velocity U_∞. The potential flow due

to these conditions is known. It yields the velocity $U(s)$ at the outer edge of the boundary layer. The boundary-layer flow is described by the velocity $u(s, y)$ parallel to the surface, where y is the coordinate perpendicular to the surface. The boundary-layer flow always begins laminar at the stagnation point $s = 0$. It is assumed that the undisturbed boundary-layer flow $u(s, y)$ is known from $s = 0$ to $s = s_s$ which specifies separation of the laminar boundary layer. The overall Reynolds number

$$R = \frac{U_\infty L}{\nu} \tag{2}$$

is based on the reference velocity U_∞ and a reference length L, normally the chord c of the wing. It can be supposed that all lengths are nondimensionalized by L, and all velocities by U_∞ ("units" U_∞ and L).

Linear stability theory shows that the amplification rates of the TS waves depend, at a position s, on the local Reynolds number R_{δ_2} according to equation (1) and the shape of the velocity profile $u(s, y)$. This shape is characterized by the shape factor

$$H_{32} = \frac{\delta_3}{\delta_2} \tag{3}$$

where δ_2 is the momentum thickness

$$\delta_2 = \int_0^\infty \frac{u}{U}\left(1 - \frac{u}{U}\right) dy \tag{4}$$

and δ_3 is the energy thickness

$$\delta_3 = \int_0^\infty \frac{u}{U}\left(1 - \left(\frac{u}{U}\right)^2\right) dy. \tag{5}$$

The same H_{32} may result from different velocity profiles. A small error is tolerated if the shape is described only by H_{32}. Different velocity profiles $u(s, y)$ with the same H_{32} may have slightly different amplification rates. This is neglected. Only one family of velocity profiles

$$\frac{u(s,y)}{U(s)} = \varphi\left(\frac{y}{\delta_2(s)}, H_{32}(s)\right) \tag{6}$$

is considered, namely the Hartree profiles. Under these assumptions, the boundary-layer stability depends only on R_{δ_2} and H_{32}. Significant values are $H_{32} = 1.57258$ for the flat plate (U = constant), $H_{32} = 1.51509$ for laminar separation, and $H_{32} = 1.61997$ for the stagnation-point flow. The profiles with $H_{32} < 1.57258$ occur in adverse pressure gradients and have an inflection point, $H_{32} > 1.57258$ occur in favorable pressure gradients.

3. Results of Linear Stability Theory

A station s with its given R_{δ_2} and H_{32} is considered. Under the assumptions discussed previously, these values are adequate for an evaluation by means of linear stability theory. This theory defines an infinite number of TS waves with different frequencies ω at each s. The solution of the well-known Orr-Sommerfeld equation yields an amplification rate for each TS wave. The most important results follow.

a) For each H_{32}, there exists a value R_N of R_{δ_2}, below which no TS wave has a positive amplification rate. Thus, the laminar boundary layer is stable for $R_{\delta_2} < R_N$

b) For lower values of H_{32}, R_N is also lower. A boundary layer profile with an inflection point is, for example, much more unstable than a profile under a favorable pressure gradient.

c) For $R_{\delta_2} > R_N$, there exist many TS waves with positive amplification rates. One of them may have the highest amplification rate.

d) For a given H_{32} a TS wave with a fixed frequency ω is not amplified for each $R_{\delta_2} > R_N$ Above another stability limit R_{N2}, this TS wave is damped again. Normally, other TS waves with other frequencies are then amplified.

e) During the development $u(s, y)$ of a boundary layer, R_{δ_2} generally increases, and H_{32} may also vary. It is very common that a certain TS wave is amplified after a position s_1 and later, after a position s_2, damped again. This is a typical result of linear stability theory.

f) The generation of higher harmonics of a TS wave is not considered in linear stability theory.

Results a) and b) can be represented in a diagram (Figure 1). All values $R_N(H_{32})$ form a line, the stability limit. Below this line or to the right of it there is no amplified TS wave, the boundary layer is stable. On the other side of the stability limit, some TS waves are amplified, others are damped. This is the unstable region. The stability limit in Figure 1 was taken from [1].

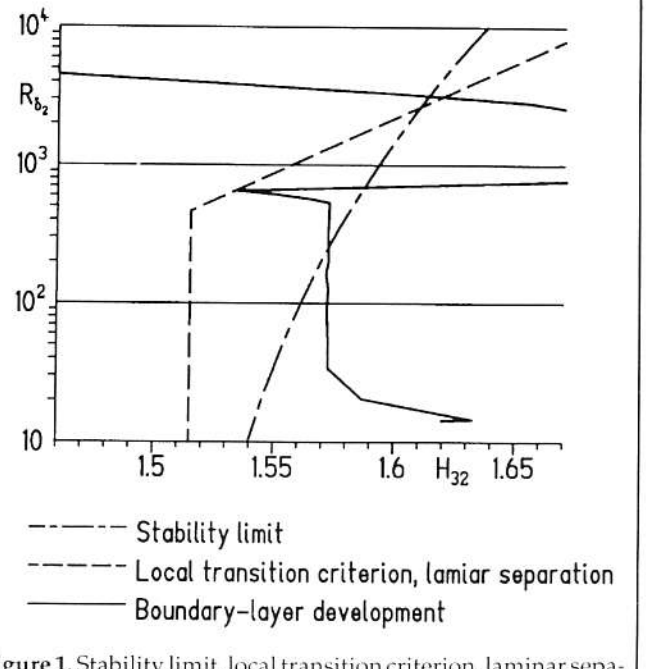

Figure 1. Stability limit, local transition criterion, laminar separation, and boundary-layer development.

4. Local Transition Criteria

At each position s the parameters H_{32} and R_{δ_2} are known. This defines a point in Figure 1. If this point is in the stable region, the laminar boundary layer is stable at s. The more

this point is to the left of the stability limit, the more unstable the boundary layer. It is conceivable that transition depends mainly on the location of this point. This would mean that a transition curve $R_T(H_{32})$ also exists in Figure 1. To test this conjecture, experimental transition data must be inserted into Figure 1. When [2] was published, only few reliable experimental data were available. They yielded a cloud of points that only showed the following tendencies:

For low values of H_{32} and, thus, low values of $R\delta_2$ the ratio R_T/R_N is large; for increasing H_{32} the ratio decreases. In the logarithmic vertical scale of figure 1, the distance log R_T— log R_N is large for low H_{32}; for increasing H_{32} the distance decreases.

Increasing H_{32} means increasing R_T, but the line log $R_T(H_{32})$ is much less steep than the stability limit.

The available data suggested the straight line $R_T(H_{32})$ shown in Figure 1. This line is, however, not the first attempt. Some modifications were necessary after many polars $c_a(c_l)$ had been computed by means of a combination of potential-flow and boundary-layer computing methods [3]. Transition criteria $R_T(H_{32})$ are "local" criteria. The formula for the line in figure 1 is

$$\ln R_T = 18.4\, H_{32} - 21.74 - 0.36\, r. \qquad (7)$$

Here, r is a rougness factor that allows surface roughness and/or free-stream turbulence to be considered. The line in Figure l is valid for $r = 0$ which means natural transition.

This criterion has been used for many years. It yielded reasonable results in many cases [4]. It was always clear, however, that it did not consider the instability history and the long transition process. Its main advantage is its simplicity.

The boundary-layer development $u(s,y)$ or $R\delta_2(H_{32})$ yields a curve in Figure 1. This representation of the boundary-layer development is very helpful. Increasing s always means increasing $R_{\delta 2}$. Although s cannot be seen from this line, it is clear that low s values are near the bottom of the diagram. The example in Figure 1 shows a vertical segment (constant H_{32}). The velocity distribution $U(s)$ of this example has a segment with constant $U(s)$ for which H_{32} = 1.57258 = constant. Boundary-layer transition can can be observed by the abrupt increase in H_{32}. In the example, the local transition criterion is used. Thus, transition occurs at the transition line. It may, however, happen that the laminar boundary layer ends at laminar separation $H_{32} = 1.51509$. In this case, an attached turbulent boundary layer can occur only if the separated flow becomes turbulent soon and reattaches again, which means a laminar separation bubble is present. The diagram of Figure l ends at $H_{32} = 1.67$. The turbulent boundary layer has much higher H_{32}-values, which are not shown in this diagram because they are not important. The line returns later in the diagram and reaches turbulent separation at $H_{32} = 1.46$.

5. The Granville Transition Criterion.

In [6], a simple criterion for the transition location was suggested already in 1953. Recently, careful transition experiments in the area of adverse pressure gradients were performed and compared with predictions from different empirical criteria [7]. It was found that the Granville criterion worked quite well in this area, much better than the local criterion previously discussed. The Granville criterion begins at the stability limit. The position s where the stability limit is reached is S_N. This means,

$$R_N = R_{\delta_2}(s_N). \qquad (8)$$

After S_N, an average form parameter

$$\bar{\lambda} = \frac{1}{s - s_N} \int_{s_N}^{s} \lambda(s)ds \qquad (9)$$

is computed. The form parameter λ is taken from the integral method of Pohlhausen for which

$$\lambda = \frac{\delta_2^2}{\nu} \frac{dU}{ds}. \qquad (10)$$

The value $\lambda = 0$ specifies the flat plate (Blasius) boundary layer; λ = -0.12, laminar separation; and λ = 0.12, the stagation point boundary layer.

For each boundary-layer development, S_N and R_N are evaluated. Then, transition is assumed to occur when $R\delta_2$ reaches

$$R_{\delta_2} = R_T = R_N + \Delta R_N(\bar{\lambda}), \qquad (11)$$

where the function $\Delta R_N(\bar{\lambda})$ is empirically adapted to experiments. A simple approximation for the function $\Delta R_N(\bar{\lambda})$ of Granville is

$$\Delta R_N(\bar{\lambda}) = 350 + 32000\bar{\lambda} + \sqrt{450^2 + 32000^2\bar{\lambda}^2}. \qquad (12)$$

This function increases with $\bar{\lambda}$, although log R_T - log R_N decreases.

Granville specified $\Delta R_N(\bar{\lambda})$ only over a small range $-0.04 < \bar{\lambda} < 0.025$. Others extended this range and introduced some modifications (see [7], for example). The Granville criterion is very simple and considers the instability history to a certain degree. If, for example, the pressure gradient becomes more adverse in the unstable region, transition is predicted later because $\bar{\lambda}$ is larger than λ at transition. This produces the correct tendency because the instability history is short in this case. The problems of the Granville criterion are:

- The Pohlhausen parameter λ does not describe the shape of the boundary layer very well;
- The average $\bar{\lambda}$ does not describe the instability history very precisely;
- There is only one function of one parameter that can empirically be adapted to experimental results.

For these reasons, a criterion was sought that can be adapted better to experimental results.

6. The New Empirical Transition Criterion

It is again supposed that the stationary boundary-layer solution $u(s,y)$ is known and the parameters $R_{\delta 2}(s)$ and $H_{32}(s)$ are computed. These results could be represented in Figure l.

It is known and also logical that the boundary layer becomes more unstable if the horizontal distance $HN\text{-}H_{32}(s)$ increases. The parameter $R_{\delta 2}$, however, also has an important effect. Transition occurs rather abruptly if the stability limit is crossed at high $R_{\delta 2}$, whereas, at low $R_{\delta 2}$ even a large distance from the stability limit promotes transition rather slowly. To be able to consider these effects empirically, a common "contribution" B to transition that depends on H_{32} and $R_{\delta 2}$ was introduced. All contributions $B(R_{\delta 2}, H_{32})$ are summed up to

$$B_i = \int_{s_N}^{s} B(R_{\delta_2}, H_{32})ds \tag{13}$$

and transition is assumed to occur when B_i reaches a limit

$$B_i = B_L. \tag{14}$$

The problem was to find a function $B(R_{\delta 2}, H_{32})$ and a value B_L such that transition is predicted well enough. It is, of course, not certain if such a criterion at all exists which covers a wide range of Reynolds numbers and boundary-layer developments. However, the function $B(R_{\delta 2}, H_{32})$ has more degrees of freedom to be adapted to experiments than the Granville criterion, and the parameters $R_{\delta 2}$ and H_{32} should allow the most important effects to be determined.

A lot of calculations and comparisons with experiments had to be performed before a good function $B(R_{\delta 2}, H_{32})$ could be specified. Experimental data from three different wind tunnels for about 20 different airfoils have been used that covered a Reynolds-number range from 1×10^5 to 9×10^6. Not all data explicitely show the transition location, but from the c_d-figures the transition locations could be evaluated to an adequate precision.

During this process, it became apparent that $B(R_{\delta 2}, H_{32})$ could not depend linearly on $H_N - H_{32}$. Very little contribution to transition seems to be present if the boundary layer is unstable but close to the stability limit. A quadratic function $B \sim (H_N - H_{32})^2$ was much better.

The effect of $R_{\delta 2}$ was underestimated in the first attempts. It was necessary to consider $R_{\delta 2}$ with a rather high exponent. The function

$$B(R_{\delta_2}, H_{32}) = 0.9225(H_N - H_{32})^2 R_{\delta_2}{}^{1.7} e^{0.612r} \tag{15}$$

in equation (13) with a limit

$$B_L = 15 \tag{16}$$

was eventually found to predict transition reasonably well over a wide range of Reynolds numbers. The last term allows surface roughness and / or free stream turbulence to be considered in a similar way as in the local criterion. The roughness factor $r = 0$ specifies smooth conditions or natural transition, $r = 4$ describes approximately surfaces with roughness like bugs or rivets, or a rather turbulent free stream.

Only the ratio 15/0.9225 of the two numbers from equations (16) and (15) is relevant.

The present criterion can be compared to the well known e^N-criterion, which uses as a contribution to transition the amplification rates of the linear theory. As mentioned in chapter 1, the e^N-criterion concerns only the very first part of the transition process and neglects many effects like the nonlinear generation of higher harmonics. Thus, it is is still an empirical procedure, and N is the only free parameter that is adapted to experiments. Different values of N have been applied.

It is admitted that the present criterion is more empirical. The objective was only to develop a simple method to predict the transition location reasonably well. More flexibility was introduced for the development of the criterion. The resulting criterion is fixed and very simple. So far, no modifications have been necessary following many comparisons with experiments not used been during the development of the criterion. The criterion increases the computing time negligibly.

7. Laminar Separation Bubbles

When the laminar boundary layer separates, a "laminar separation bubble" (abbreviated by "bubble") may occur. The phenomenon of the bubble is very significant in many cases, mainly for Reynolds numbers below 2×10^6. It may cause a considerable increase in drag, the "bubble drag" .

The boundary-layer method [2] that is used in the present paper switches immediately after laminar separation or transition to the turbulent formulas for skin friction and energy dissipation. However, these turbulant formulas differ little from the laminar ones as long as $R_{\delta 2}$ is low. This region can be understood as a "bubble analog" [2]. Until recently this bubble analog was used only to issue a bubble warning. The experiments concerning bubbles were not systematic enough to allow a correlation between the bubble analog and the bubble drag.

Much theoretical research has been done in the meantime with respect to bubble drag, for example [10], [11]. The models of the bubble in these papers require considerable computing time and the results turned out to be not satisfying in many cases. One of the most difficult problems is that the bubble drag depends on the instability history in front of the bubble. After this instability history was evaluated in the new transition criterion, and new experimental results became available, mainly from the wind tunnels in Stuttgart and Delft, [7], [9], and [12], another attempt was made to correlate the bubble drag with the bubble analog.

The bubble analog is defined as the region between the end s_s of the laminar boundary layer and the location s_A where the shape factor H_{32} reaches a value H_{BE} (for bubble end). Within this region, the potential-flow velocity $U(s)$ decreases. The parameter

$$\Lambda_A = \frac{U(s_S) - U(s_A)}{U(s_S)} \tag{17}$$

is the relative velocity decrease.

For long time, a constant value $H_{BE} = 1.6$ was used. More recently, it was found that a decreasing $H_{BE}(s)$ resulted in a better correlation. This takes into account that reattachment occurs with a lower H_{32} for a longer bubble. After several attempts, it was determined that the function

$$H_{BE}(s) = 1.54 + 0.07\frac{\sqrt{1+4\xi^2}-1}{2\xi} \tag{18}$$

with

$$\xi = \frac{1}{15}\left(\frac{s - s_S}{\delta_{2s}} - 110\right) \tag{19}$$

yields reasonable values of ΛA It is important to consider s–s_s relative to the momentum thickness δ_{2s} at the beginning of the bubble. The function $H_{BE}(s)$ is shown in Figure 2.

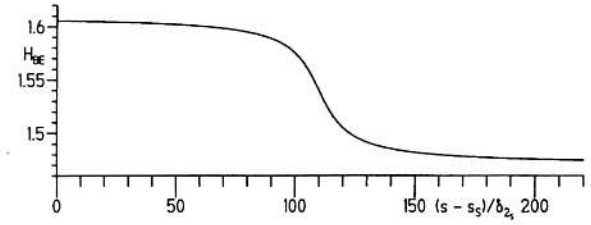

Figure 2. The function H_{BE}.

The integrated contributions to transition at s_s

$$B_S = B_i(s_S) \tag{20}$$

and the local Reynolds number at s_s

$$R_S = \frac{U(s_S)\delta_{2S}}{\nu} \tag{21}$$

are additional important parameters. It was therefore tried to find a function

$$\frac{\Delta\delta_2}{\delta_2(s_A)} = \Phi(\Lambda_A, B_S, R_S) \tag{22}$$

by which the increase in δ_2 due to the bubble could be predicted. Of course, a negative Φ is not allowed. The energy thickness δ_3 is assumed to remain unchanged. A positive $\Delta\delta_2$ thus decreases H_{32}.

The procedure to find an adequate Φ was again completely empirical. Because separation bubbles are extremely sensitive to the flow quality of wind tunnels, it is clear that Φ can yield only rough approximations if results from different wind tunnels are considered. However, a rough estimate of the bubble drag is better than merely a warning of the possible presence of bubbles.

The function which so far yields reasonable estimates of the bubble drag is

$$\Phi = \left(0.09(30 - B_S)(\ln R_S - 2.5) + \frac{12}{1 + 0.4B_S^2}\right)h\Lambda_A - 0.05. \tag{23}$$

Here, one additional parameter h appears. It was found that a bubble is less significant if it is located near the trailing edge and even more so if U_s is low. If $x_A = x(s_A)$ is the chordwise location of the end of the bubble analog, and x_{TE} is the trailing edge, then

$$\begin{aligned} h &= 1 && \text{if } x_A \le x_{TE} - x_h, \\ h &= \frac{x_{TE} - x_A}{x_h} && \text{if } x_A > x_{TE} - x_h, \end{aligned} \tag{24}$$

where

$$\begin{aligned} x_h &= 0.02 && \text{if } U_S \ge 1.3, \\ x_h &= 1.32 - U_S && \text{if } U_S < 1.3. \end{aligned} \tag{25}$$

Only if x_A is near the trailing edge and U_s is low, can h be smaller than 1.

8. Examples

The first example was used during the development of the transition criterion. The experimental results are taken from [7]. The airfoil which was used for these experiments is shown in Figure 3. It exhibits a long segment from 15 to 70 percent chord with moderate adverse pressure gradient. In this region the transition location is very sensitive to the angle of attack a for $\alpha = 0°$ to $\alpha = 5°$. Near 15 percent chord the velocity distribution has a slight bump. This

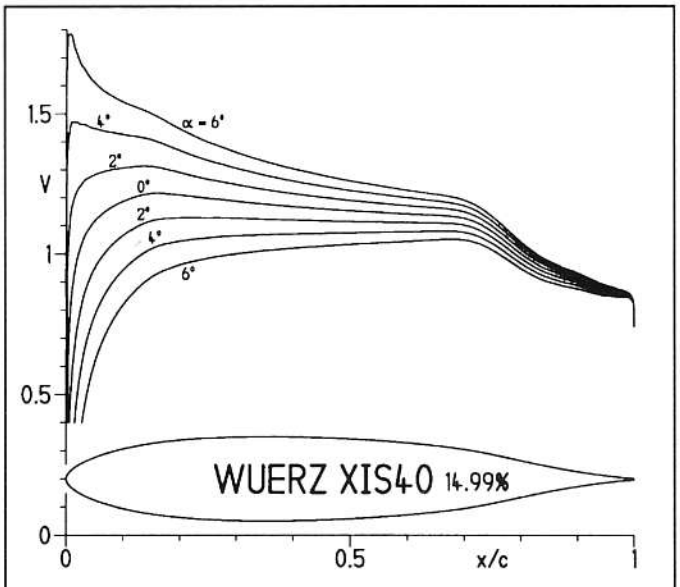

Figure 3. Potential-flow velocity distributions for the Würz XIS40 airfoil.

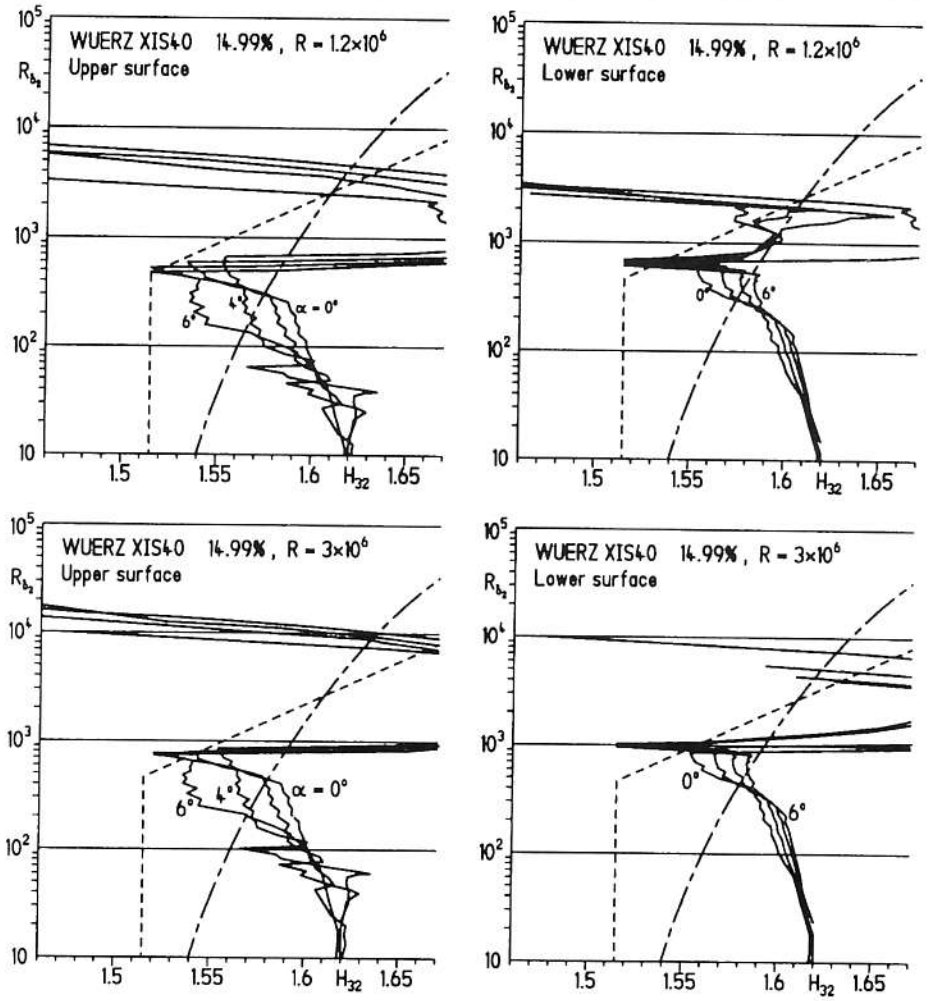

Figure 4. The boundary-layer developments for the velocity distributions shown in Figure 3.

changes the shape factor, which becomes obvious in the boundary-layer development plot which is shown in Figure 4 for two Reynolds numbers, $R = 1.2 \times 10^6$ and $R = 3 \times 10^6$. This figure deserves careful interpretation.

- The boundary-layer-developmant curves show some oscillations. The oscillations are even large in the lower part of the diagrams. This shows that the airfoil coordinates are not exactly smooth, even though the airfoil shape looks smooth. Some irregularities near the leading edge can, however, be seen in the velocity distributions (figure 3). The boundary layer calculation "enlarges" these irregularities. Even in the area where the velocity distributions look smooth, some oscillations can be seen in the boundary-leyer development. The boundary-layer computation is, thus, a good check for the smoothness of the airfoil coordinates.
- The change in the shape factor due to the bump in the velocity distribution near 15 percent chord shows up at a relatively high $R_{\delta 2}$. Note that the arc length s is not represented linearly in this diagram. Near the leading edge $\log R_{\delta 2}$ changes greatly with s; later on, much less. The leading edge region is, thus, enlarged in this diagram.
- If the Reynolds number is changed from R_1 to R_2, the laminar part of the boundary layer development is merely shifted in the vertical direction. The amount of this shift is $\log \sqrt{R_2/R_1}$.
- The new transition criterion was used in figure 4, the line for the local criterion (7) is also shown. It can clearly be seen that transition occurs, according to the new criterion, before the local criterion is reached if a long instability history is present; it occurs much later if a short instability history is present. The latter case is most obvious on the lower surface. Even for $R = 3 \times 10^6$, the curves for the lower surface reach the laminar separation. Separation bubbles must be expected in this case.
- In this diagram, transition according to the new criterion is not too far from the old local criterion. It should be remembered, however, that the differences are much larger with respect to the arc length s.

The c_a/c_l-polars are shown in Figure 5 for the same Reynolds numbers as in Figure 3 The most significant result is that the transition locations (in the right part of the diagrams) from the new criterion show the same tendency as the experiment, which is not true for the locations from the old criterion.

The locations from the new criterion always show earlier transition than the experiment. This is due to the fact that only the fully developed turbulent boundary layer is detected in the experiment whereas the computation switches to the turbulent skin-friction and energy-dissipation equations once the laminar boundary layer ends. This location is then defined as the transition location. The difference between the predicted and the measured locations is larger for low Reynolds numbers because the transitional region is longer. The largest differences must occur if a separation bubble is present. The computed transition location is the beginning of the bubble, the experimental one at the end.

Based on these facts the predicted and measured locations agree quite well. The differences between the locations from the new criterion and the experimental results are smaller for the higher Reynolds number, as they should

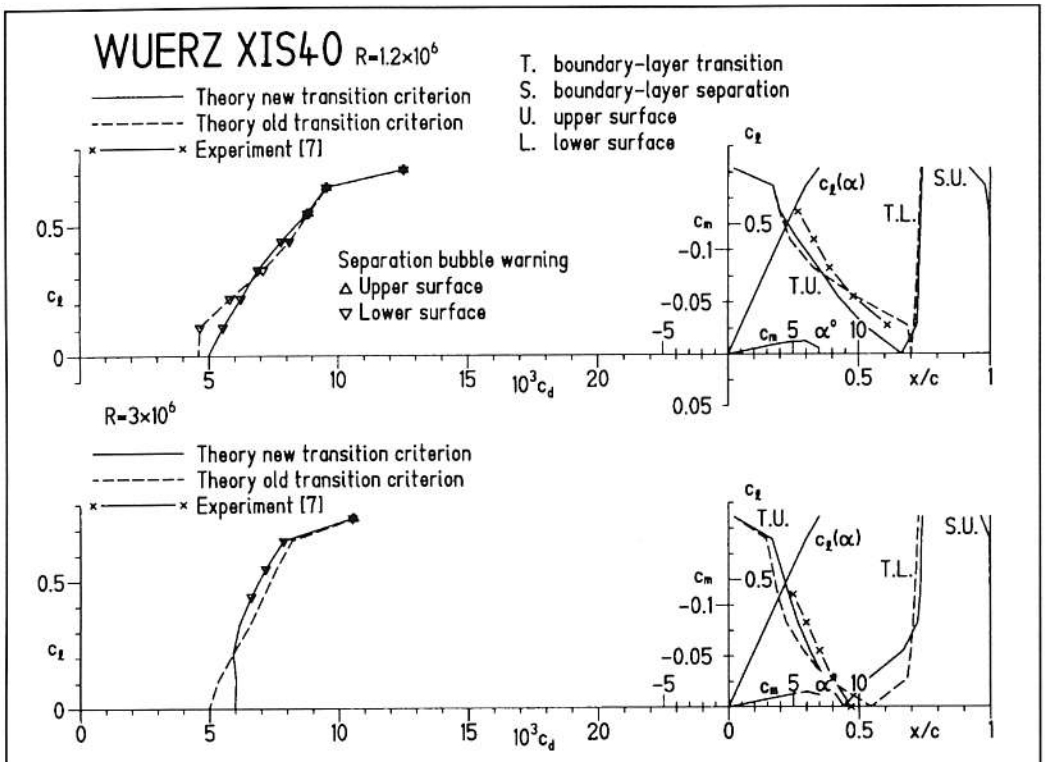

Figure 5. Section characteristics of the Würz XIS40 airfoil..

be.

The next example concerns the TL 100 airfoil [8]. It is shown in Figure 6 along with various velocity distributions, the section characteristics for $R = 2 \times 10^6$ in Figure 7 [9]. This example was used to check the new criterion, not to develop it. The transition locations are predicted quite well. Only near the upper limit of the low-drag range is transition predicted slightly too far aft. This is the region where transition depends strongly on the angle of attack. The drag polars agree well.

The intention of [8] and [9] was to investigate why the e^N-method needs different N-factors in different cases. This example is therefore of special interest. For this airfoil in this wind tunnel, good correlation between theory and experiment was obtained for N-factors from 13 for $R = 1 \times 10^6$ to 10.5 for $R = 3 \times 10^6$. It was assumed that the increase in turbulence level with tunnel speed leads to the decrease in N-factor with Reynolds number. Additional testing, for example, using two model chords to obtain the same Reynolds number at different tunnel speeds, to corroborate this assumption has not been performed to date.

All other Reynolds numbers from [8] have also been used to validate the new transition criterion and the empirical bubble drag. The comparisons are all similarly favorable.

The third example concerns the S805 airfoil [12] which was tested in the low-turbulence wind tunnel of the Delft University of Technology from $R = 0.5 \times 10^6$ to $R = 2 \times 10^6$. These results are of special interest with respect to the bubble drag. The S805 airfoil along with two velocity distributions is shown in Figure 8. The beginning of the pressure recovery on the upper surface is rather abrupt which promotes the formation of bubbles. The experimen-

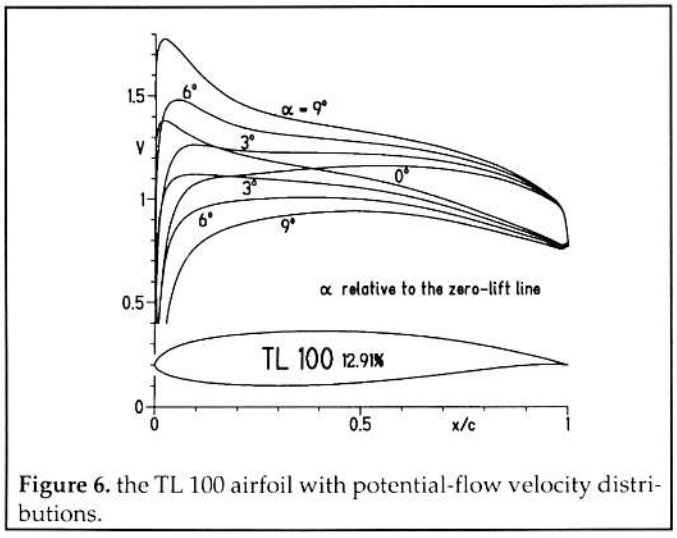

Figure 6. the TL 100 airfoil with potential-flow velocity distributions.

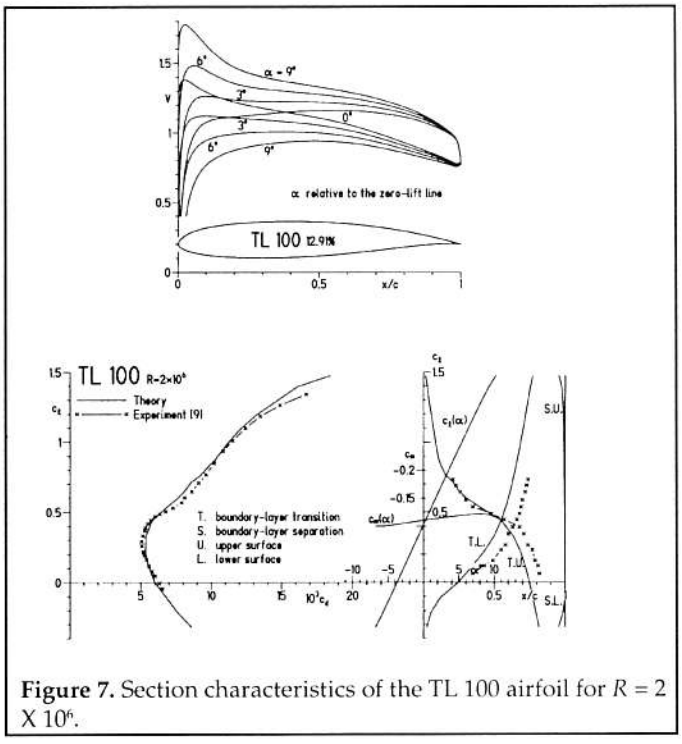

Figure 7. Section characteristics of the TL 100 airfoil for $R = 2 \times 10^6$.

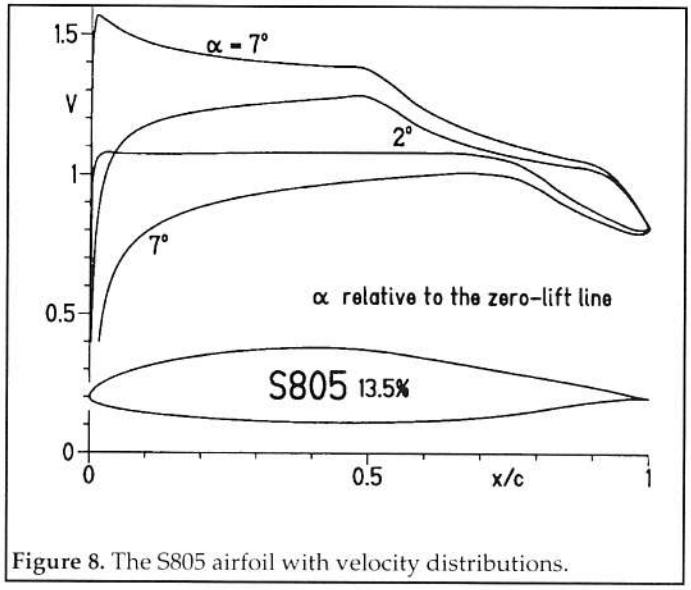

Figure 8. The S805 airfoil with velocity distributions.

tal drag polars for $R = 0.5 \times 10^6$ and $R = 0.7 \times 10^6$ are shown in Figure 9 and compared with the computed polars with and without bubble drag.

The polars with bubble drag agree much better with the experiments, although the bubble drag is a little overpredicted for $R = 0.5 \times 10^6$. The difference between the predicted and the experimental transition locations is not constant in these comparisons. This may indicate that the bubbles become on the upper surface shorter with increasing α, on the lower surface longer.

The fourth example concerns the E 387 airfoil which was designed around 1960 for model airplanes having Reynolds numbers above $R = 2 \times 10^5$. The airfoil along with three velocity distributions and the polars for $R = 1 \times 10^5$ and $R = 2 \times 10^5$ are presented in Figures 10 and 11. The experiments have been performed in Delft, for $R = 2 \times 10^5$ on two separate occasions. The two sets of experiments agree quite well, although they are not identical.

9. Concluding Remarks

The computational results from the combined application of potential-flow and boundary-layer methods become more and more valuable. One remaining question is the difference between wind-tunnel and free-flight conditions. In one of the cited examples, it was necessary to vary

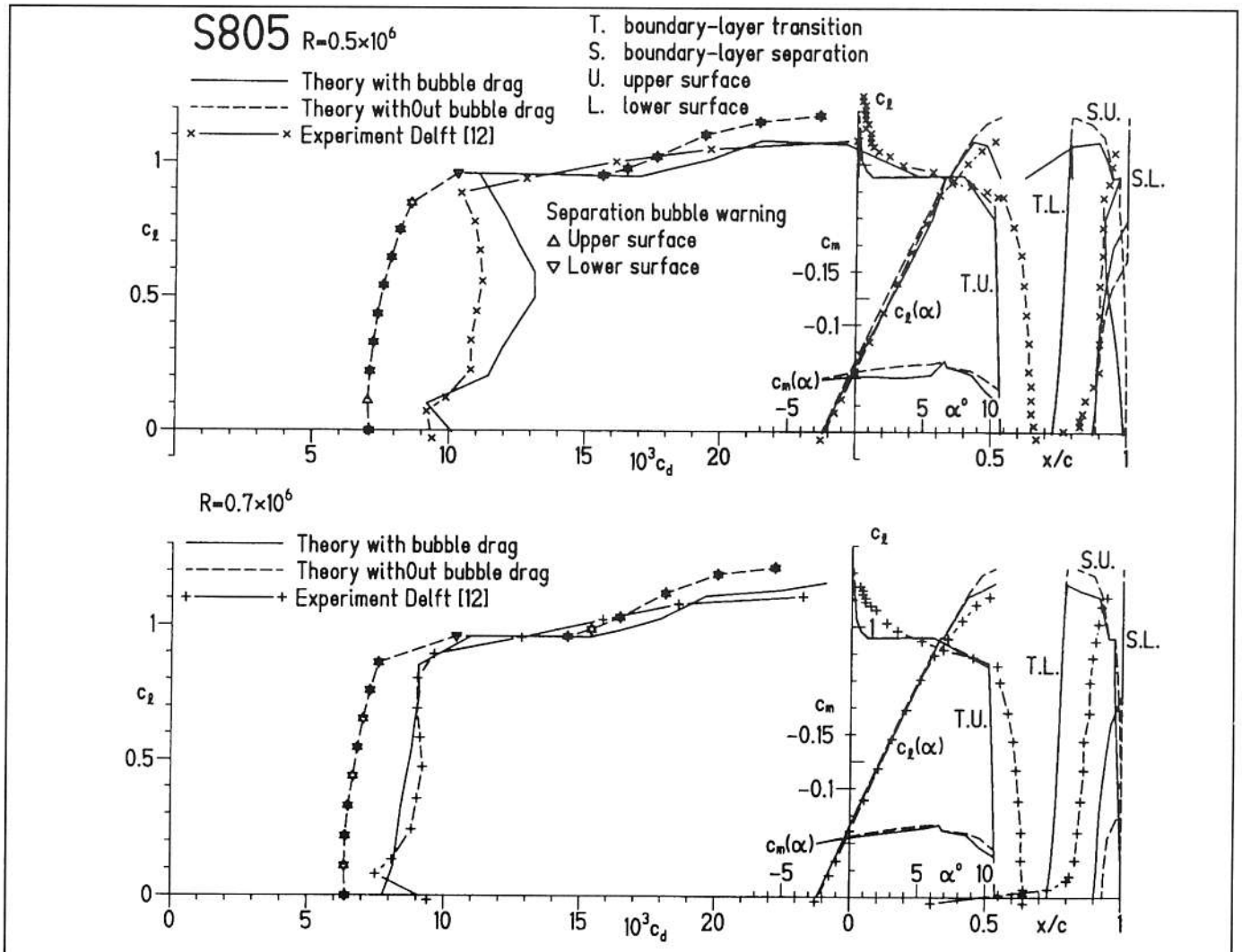

Figure 9. Section characteristics of the S805 airfoil for $R = 5 \times 10^5$ and $R = 7 \times 10^5$.

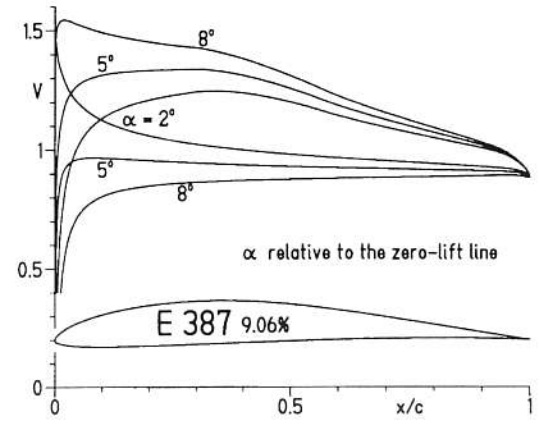

Figure 10. Airfoil E 387 with potential-flow velocity distributions.

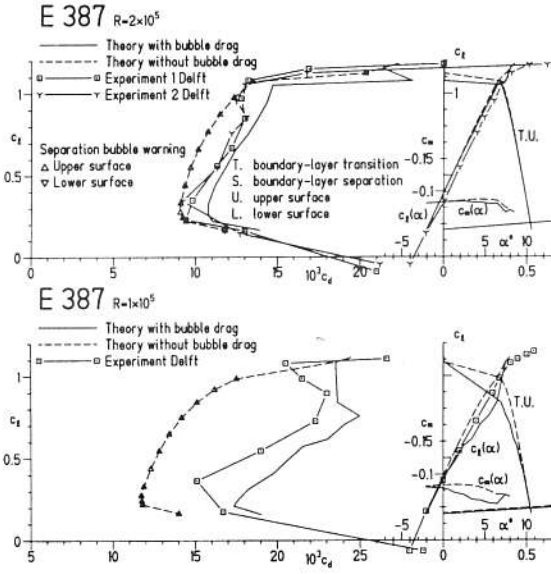

Figure 11. Section characteristics of airfoil E 387 for $R = 1 \times 10^5$ and $R = 2 \times 10^5$.

the e^N-criterion considerably to obtain good correlation with the wind-tunnel results. The required variation in N-fractor was attributed to the variation in the turbulence level of the tunnel with tunnel speed. This result suggests two possibilities.

If the tunnel speed really has such a strong effect on the N-factor, this effect must be determined for each wind tunnel, and the experimental results cannot be applied to the free-flight conditions without a prediction of the differences due to the different conditions. Theoretical methods should be very helpful for this extrapolation to free-flight conditions.

If the variation of the N-factor in the e^N-criterion is inherent in the criterion itself, the development of new transition criteria is justified.

References

[1] *Wieghardt, K.:* Die Berechnung ebener und drehsymmatrischer Grenzschichten mit kontinuierlicher Absaugung, Ing.-Arch. 22 (1954), pp. 369 - 377.

[2] *Eppler, R.:* Praktische Berechnung laminarer und turbulenter Absauge-Grenzschichten, Ing.-Arch 32 (1963), pp. 221- 245.

[3] *Eppler, R.:* Laminarprofile fur Reynoldszahlen grol3er als 4 x 106, Ing. Arch. 38 (1969), pp. 232 - 240. English translation: Office of International Operations N 69 - 28178, 1969.

[4] *Eppler. R.:* Airfoil Design and Data, Springer-Verlag (1991).

[5] *Somers, D. M.:* Subsonic Natural-Laminar-Flow Airfoils. Natural Laminar Flow and Laminar Flow Control, Barnwell, R. W., Hussaini, M. Y., eds., Springer-Verlag New York, Inc. 1992, pp. 143- 176.

[6] *Granville, P. S.:* The Calculation of Viscous Drag of Bodies of Revolution, Navy Department, The David Taylor Model Basin, Report No. 849 (1953).

[7] *Wurz, W.:* Hitzdrahtmessungen zum laminar-turbulenten Stromungsumschlag in anliegenden Grenzschichten und Abloseblasen sowie Vergleich mit der linearen Stabilitatstheorie und empirischen Umschlagkriterien, Dissertation Universitat Stuttgart 1995.

[8] Lutz, T.: Profilentwurf zur Korrelation des kritischen Anfachungsfaktors bei niedriger Anstromturbulenz. Report Institut fur Aerodynamik und Gasdynamik, Universitat Stuttgart 1996.

[9] *Wurz, W.:* Polarenmessungen am Profil TL-100 zur Korrelation des n-Faktors fur den Laminarwindkanal. Report Institut fur Aerodynamik und Gasdynamik, Universitat Stuttgart 1996.

[10] *Dini, P., Maughmer, M. B.:* A Locally Interactive Laminar Separation Bubble Model. Journal of Aircraft 31 (1994), pp. 802 - 810.

[11] *Drela, M., Giles, M. B.:* Viscous-Inviscid Analysis of Transsonic and Low-ReynoldsNumber Airfoils. AIAA Journal 25 (1987), pp. 1347- 1355.

[12] *Somers, D. M.:* Design and Experimental Results for the S805 airfoil. National Renewable Energy Laboratory, Golden CO., Report NREL/SR-440-6917, 1997.